JOURNAL OF FORENSIC SCIENCES

J Forensic Sci, July 2011, Vol. 56, No. 4
doi: 10.1111/j.1556-4029.2011.01747.x
Available online at: onlinelibrary.wiley.com

TECHNICAL NOTE

CRIMINALISTICS

Bjørn K. Alsberg,[1] *Ph.D.; Trond Løke,*[2] *M.Sc.; and Ivar Baarstad,*[2] *M.Sc.*

PryJector: A Device for *In Situ* Visualization of Chemical and Physical Property Distributions on Surfaces Using Projection and Hyperspectral Imaging*,†

ABSTRACT: Traditional forensic methods that highlight the spatial distribution of properties such as blood and fingerprints have two main disadvantages: they often apply chemicals that may influence further analyses, and they cannot easily be modified to search for new compounds/properties. A new instrument (called PryJector) avoids these problems by dynamically projecting back onto the surface under study spatially distributed information of compounds/properties (chemical images) obtained from multivariate analysis of hyperspectral images. Selectivity to target compounds/properties is ensured by multivariate modeling which makes the instrument much more flexible compared to traditional methods. The functionality of the PryJector is demonstrated in an application related to the detection of counterfeit pharmaceuticals where compounds otherwise indistinguishable to the human eye are made clearly visible by projection of false-colored chemical images. The PryJector is shown to be a noninvasive and very flexible instrument for highlighting spatial distributions of various compounds/properties.

KEYWORDS: forensic science, hyperspectral analysis, *in situ* visualization, chemical imaging, chemical images, projection, chemometrics, near-infrared spectroscopy, PryJector

Highlighting the *in situ* spatial distribution of chemical and biological information such as the presence of blood (1), saliva (2), semen (3), narcotics (4), and gun powder (5–7) on objects from crime scenes has become an important tool in forensic analysis. Existing techniques typically achieve this effect by using fluorescence or applying chemiluminescent dyes onto object surfaces that react with target compounds. Fluorescence in the visible part of the spectrum is often achieved by illuminating the surface with ultraviolet light (8). When inspected, areas on the objects containing the target compounds or properties emit visible light and are easily seen by the investigator. However, the use of dyes and other chemicals for highlighting target compounds or properties has two main disadvantages. The first one is that the dyes may alter the material such that further analyses are made more difficult. For instance, when luminol (9) is used for detection of blood, it may reduce the amount of DNA that can be recovered. The second important disadvantage with many standard techniques is that they are usually very difficult to modify to achieve selectivity for a new property or compound. Therefore, a more flexible, general, and noninvasive approach is needed. Here, we present an alternative approach based on using a novel combination of existing technologies: chemometric analysis of spectroscopic profiles at different spatial locations (hyperspectral imaging) performed dynamically and false-color projection of the detection/classification result back onto the scene to highlight what is otherwise invisible to the naked eye.

Detection of various chemical compounds or properties on surfaces can rapidly be performed using hyperspectral technology. Multispectral and hyperspectral cameras record scenes at multiple wavelengths which result in a three-dimensional (3D) data array, the hypercube, where a continuous and detailed radiance or reflectance spectrum for each pixel is stored. Such spectra may contain chemical, physical, and/or biological information that can be extracted using various mathematical and statistical techniques. Of particular interest is the use of chemometric methods (10,11) for multicomponent analysis and model calibration. These computational methods are used to generate so-called chemical images that show the spatial distribution of chemical and physical information. Hyperspectral technology originated within the field of remote sensing; however, it is increasingly being used in different areas such as chemistry, biology, and medicine because it effectively combines imaging with spectroscopy.

Most existing hyperspectral cameras are based on either push-broom spectrograph or wavelength filtering technology. For push-broom scanners like the one used in this article, the camera fore optic is imaging the scene onto a slit that defines the linear field of view (FOV) of the instrument. It then collimates the light before the dispersive element. The dispersive element (in our case a transmission grating) separates the light into different wavelengths that are focused onto a 2D detector array by means of an objective lens. The net effect of the optics is that each pixel column on the

[1]Department of Chemistry, Norwegian University of Science and Technology (NTNU), Høgskoleringen 5d, N-7491, Trondheim, Norway.
[2]Norsk Elektro Optikk AS, P.O. Box 384, N-1471, Lørenskog, Norway.
*Trond Løke and Ivar Baarstad both work in the company NEO who have built the hyperspectral camera and PryJector setup from specifications provided by Bjørn K. Alsberg. Professor Alsberg is not associated with NEO.
†Funding provided by the Norwegian Research Council and the Department of Chemistry at NTNU.

Received 31 Aug. 2009; and in revised form 27 May 2010; accepted 5 June 2010.

© 2011 American Academy of Forensic Sciences

detector array corresponds to a spatial pixel position in the scene, and the different pixels in a particular column are receiving photons from a specific wavelength interval (spectral band), thus in total generating a full spectrum for each spatial pixel position.

To get a 2D image of the scene, some sort of scanning is needed, typically implemented by translation of the camera (or the scene) or rotation of the camera. The resulting image data can be considered as multiple separate monochrome 2D images of the scene (one for each spectral channel) or alternatively that every pixel in the image contains one full radiance or reflectance spectrum.

For this type of scanner, the full spectrum in a particular pixel is acquired simultaneously, ensuring the integrity of the spectral data.

The other main approach for hyperspectral imaging is based on using a tunable bandpass filter in front of the camera where a whole 2D image for each wavelength is recorded at a time. This slices the hypercube in a different way from using a push-broom scanner camera. Each [spatial × spatial] matrix slice is acquired by stepping the bandwidth filter one wavelength after another. Examples of bandpass filters used in hyperspectral cameras are the acousto-optical tunable filter (AOTF; [12]) and the liquid crystal tunable filter (LCTF). AOTF is a solid-state electronically tunable bandpass filter where acoustic waves produce index of refraction changes (13–15). The LCTF is using a stack of polarizers and tunable retardation liquid crystal plates (16–19) to achieve bandpassing of the incoming light.

Over the last 10 years, there has been a significant increase in the number of articles published using chemical imaging for forensic purposes. A majority of these contributions have been in the area of fingerprint detection (20–32). In most of these cases, chemical imaging has been used to enhance weak and borderline fingerprints already treated with traditional methods, such as ninhydrin and cyanoacrylate. In Ng et al. (21), Fourier Transform Infrared-based chemical imaging was used to detect various substances contained in fingerprints, such as explosives, gunshot residues, and illegal substances. Detection of explosive residues in fingerprints was also demonstrated in Emmons et al. (24) using Raman chemical imaging. Examples of other forensic applications using chemical image analysis are classification of man-made bicomponent fibers (25), document analysis where spectra were used to determine the sequence of intersecting lines produced by ballpoint pens and laser printers (26), analysis of paints, inks, and firearm propellants (27) in the UV–Vis–NIR and IR regions, the detection of mass graves using remote sensing (airborne and satellite imagery) in the UV–Vis–NIR range (28), the use of Raman imaging to detect different types of condom lubricant compounds (29), and the detection and visualization of foreign matter in human tissue (30) using near-infrared chemical imaging. In addition, the application of chemical imaging techniques such as time-of-flight secondary ion mass spectrometry has also been reported in the literature, here for detecting various bioagents (31). This work also demonstrated the use of energy dispersive X-ray spectroscopy for detection of bioagents that enables elemental analysis and chemical characterization. Most of the articles published are not using any chemometric or multivariate methods for analysis. However, among those that do, principal component analysis (PCA) and hierarchical clusterings are the most commonly used methods.

Regardless of the working principle, once the spectra from the hypercube become available, multivariate analysis can take place. Both unsupervised (explorative) and supervised (classification and regression) modeling are possible. The generated chemical image is typically presented as a classification of different compound classes or their estimated concentration levels. The usual way to view the chemical image is on a computer screen. However, for applications where interactive manual inspection of a surface is of importance, this may be a hindrance. A more intuitive approach is to make the chemical information computed from the spectra dynamically available onto the surface under inspection and aligned with the structural features from where it originated. A way to accomplish this is to use an ordinary computer projector or a laser to dynamically project and update the calculated chemical images back onto the original surface. To our knowledge, no other chemical imaging systems reported in the literature make use of this unique feature that forms the core idea behind the new instrument here referred to as a PryJector. False coloring can be used to indicate different classes or levels of concentrations of a compound. The effect is that otherwise invisible features on surfaces to the naked eye become clearly visible *in situ*.

Of particular interest is using a PryJector for rapid updating of chemical information on surfaces. Many real-time applications involving handling of objects on surfaces would benefit from such an instrument. The scan speed achievable with this first prototype system (7.5 cm/sec) should be adequate for many applications, and three to four times higher scan speed is possible with currently available sensor technology, making such a system potentially useful in real-life applications.

The aim of this article is to (i) demonstrate how the PryJector technology works and (ii) investigate how it can facilitate manual, interactive, and *in situ* forensic investigations of surfaces by utilizing the key advantages of the new instrument: intuitive visualization of chemical information on surfaces and increased flexibility with respect to new target properties to visualize. The core property of the PryJector is dynamically updated projection of false-colored chemical images onto surfaces that are registered to the features under investigation.

Technology

A PryJector can be assembled into different configurations based on its usage and type of hyperspectral system. In this article, we

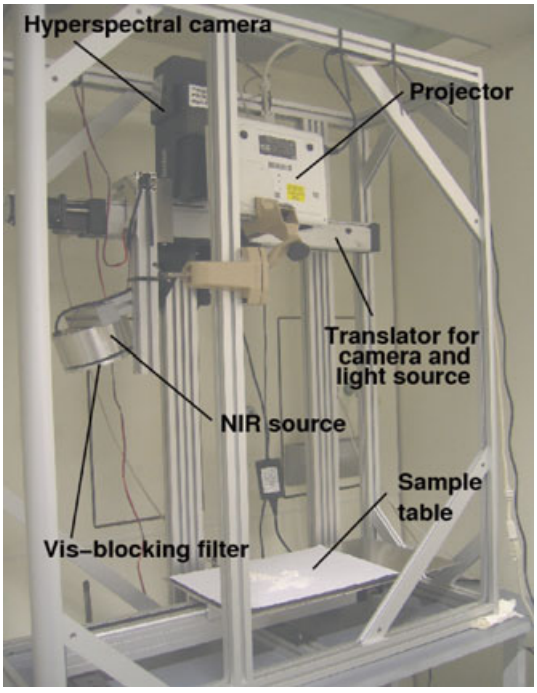

FIG. 1—*The table top version of the PryJector.*

focus on a table top version using push-broom technology. The basic setup of the experiment is shown in Fig. 1 where the camera and light source are mounted on a common translation stage. This configuration is designed to study objects positioned on a flat table, such as clothes, documents, food, pharmaceuticals, and art work. Another possible configuration for a PryJector is based on a rotation stage that is useful for scanning larger scenes. Only the table top version will be discussed here.

In this experiment, a HySpex SWIR-320i hyperspectral camera from Norsk Elektro Optikk AS was used. The instrument is a push-broom scanner based on an InGaAs focal plane array (FPA) with a spectral range of 930–1670 nm. The number of across track spatial pixels is 320, and the number of recorded wavelengths is 148. The spectral sampling interval is 5 nm, and the pixel FOV is 0.75 mrad. The frame rate for the system used is 100 fps where one frame on the FPA contains all the 148 wavelength bands from a single spatial line (320 pixels). The HySpex camera was spectrally and radiometrically calibrated before the experiment by means of narrow band laser sources (spectral calibration) and a calibrated integrated sphere (radiometric calibration). The sensor dark offset matrix is automatically acquired for each image by means of a built-in electromechanical shutter. The spectra generated by such an instrument are therefore representing the absolute radiance in $W/(m^2$ nm sr). InGaAs arrays inherently suffer from a certain fraction of bad pixels, such as hot, dead, and noisy pixels (typically in the range 0.5–1%). These pixels are characterized in beforehand and interpolated using the nearest neighbors in the spectral direction.

A custom-made 150-W lamp with a high light intensity both in the visible and infrared (400–2500 nm) region is used to illuminate the samples. To minimize distraction from this light source and enhance contrast when performing projection (in the visible part of the spectrum), a long wave pass filter with cut-on at 850 nm was used to almost completely block all wavelengths from below 800 nm. Attached at the same height as the camera is an ordinary color computer projector (Hewlett-Packard MP3222 with XGA, 1024×768 and 2000 lumens; Hewlett-Packard Co., Palo Alto, CA) that projects a color image down onto the total working space of the sample table (23.5×60.0 cm). The projector is updating the chemical images continuously onto the table/samples using false colors. No special preference for color combinations is made as long as they appear different from each other and the surrounding environment. Because of the brightness of the projected image, however, there are no problems with visually discriminating a point which is highlighted by the projector from one which is not. Here, we have decided to use basic colors such as red, green, blue, and yellow for the different classes. Alignment of the projection system with the hyperspectral image (or scene) has only been performed with limited precision (typically up to a few pixels misregistration, depending on the position in the FOV). Coregistration with precision at the pixel (or subpixel) level is indeed possible, but was not the main focus of the current work.

The camera is located 100 cm from the scene, yielding a pixel size of 0.75 mm. At 100 Hz scan rate, this corresponds to a scan speed of 7.5 cm/sec. The integration time used was typically 1 msec, whereas the frame time was 10 msec (corresponding to 100 Hz scan rate), so if a camera with faster readout is used, the scan speed can in principle be increased by a factor 10 with the same light level and intensity. Similar InGaAs FPAs with three to four times higher frame rate are currently available.

For the PryJector setup, the camera and light source are mounted on the translation stage 1 m above the scene. The scene and projector are static. The camera and projection system are operating continuously in both scan directions, ensuring a rapid update of the projected classification results.

It might be possible in future developments of the PryJector to significantly increase the scanning speed by employing a rotary mirror setup instead of scanning the camera and light source.

The HySpex data acquisition software has the option to perform real-time correction of the images. The real-time correction procedure includes subtraction of dark offset, spectral and radiometric calibration as well as bad pixel interpolation before storing and/or analyzing the data on the fly. The output signal available from each spatial pixel in real time is proportional to radiance and can be analyzed directly without need for a time-consuming postprocessing step to generate calibrated image data/spectra.

The recorded frames from the HySpex SWIR-320i are sent to a quad core Intel computer running at 2.66 GHz (2 GB RAM; Intel Corp., Santa Clara, CA) and analyzed by the multivariate software that generates the chemical images. The data analysis software for the system is currently written in Matlab (The MathWorks, Inc., Natick, MA), whereas the HySpex data acquisition software is written in Visual C++.

In summary, our push-broom system is different from other existing hyperspectral system in the following ways:

- It is in a continuously scanning mode.
- While in this mode, the chemical image (really the chemical line image) is continuously computed and updated.
- This continuous operation is connected to an ordinary computer projector that projects on-the-fly computed false-colored chemical images back onto the surface.
- The projected image is registered to the original features on the surface.

This dynamic projection of the chemical images provides the chemical information *in situ* to the user while manually inspecting the surface. This is a much more intuitive way of providing the information than inspecting an off-line image on a computer monitor. The core idea here is to facilitate how humans can interact with surfaces in the most intuitive and informative way. Thus, the human scale is an important element of the PryJector system. If a hyperspectral camera is used to inspect microscopic samples or structures of large areas, using back projection becomes unnecessary and meaningless. In such cases, inspecting a computer screen is sufficient. However, in many applications, where the manual and interactive inspection of a surface is performed by a human, the PryJector is designed to provide information about the surface distributions of chemical and physical properties in a way which is natural for us.

Methods and Materials

Data Set

To investigate the usefulness of the new instrument, an application related to the pharmaceutical industry is presented. In various developing countries, there is high risk of obtaining counterfeit pharmaceuticals which can result in medical problems or death (33). The ability to rapidly distinguish real from fake medicines in forensic and medical applications is therefore very important. Here, we have focused on distinguishing different tablets that to the naked eye appear very similar. The literature (34) has reported positive results on using Raman and infrared spectroscopic techniques to detect counterfeit pharmaceuticals. Here, we use a similar approach to investigate the applicability of a PryJector instrument.

The data set used consists of four different types of organic nonprescription pharmaceuticals in tablet form that are all used in pain

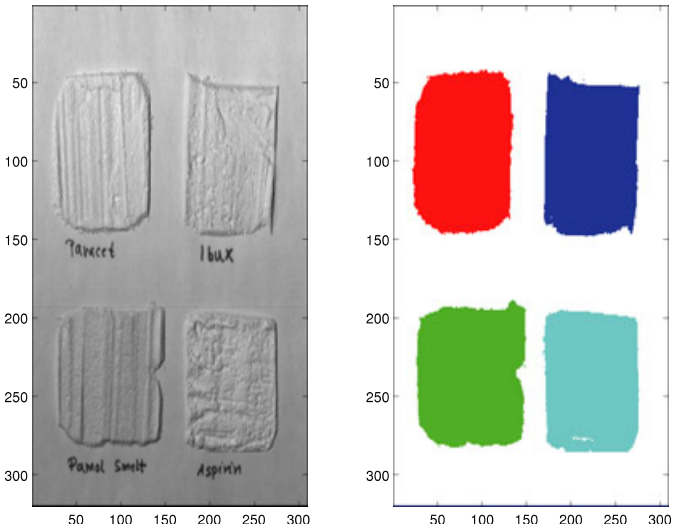

FIG. 2—*Image of the calibration data. Each rectangular area corresponds to one of the four pharmaceuticals used (Paracet, Ibux, Pamol Smelt, and Aspirin) in powder form.*

relief: Paracet (active compound is Paracetamol), Pamol Smelt (active compound is also Paracetamol), Ibux (active compound is Ibuprofen), and Aspirin (active compound is acetylsalicylic acid). Thus, the recorded pixels from the hyperspectral camera must be separated into five different classes where the fifth class corresponds to the background.

Four different hyperspectral images have been recorded: Image 1 (Fig. 2) that is used for calibration of the classification models and Images 2, 3, and 4 are used for testing. In the calibration data set in Image 1, the tablets are crushed into powder form. The reasons for this are (i) crushing and good mixing of the powders improves on any possible heterogeneity on tablet surfaces, (ii) powders have much less specular reflectance than observed on smooth tablet surfaces, and (iii) powders can easily be distributed evenly over a larger area with a simple geometry (like a rectangle) which makes it easier when assigning class membership to pixels. None of the chosen tablets for this experiment contained a separate protecting coating layer which otherwise would have made crushing to powder form much less useful.

Data Analytical Methods

To build predictive multivariate classification models, two different methods were used: discriminant partial least squares (DPLSR) regression (10) and a simplified version of the *k*-nearest neighbor (*k*-NN) classification method (35) using the spectral angle mapper (SAM; [36]) as distance measure. Here, the *k*-NN method is only used with the $k = 1$ setting, that is, class membership of a new input vector is determined by its SAM distance to its nearest neighbor to one of the five class center vectors. The DPLSR method is based on the PLS2 algorithm using multiple dependent variables (referred to as the *Y*-variables). These *Y*-variables are contained in a matrix which encode the different class memberships for each object. The *X*-matrix contains the independent variables, that is, the spectral intensities at different wavelengths, as columns. A binary encoding is typically used where the *Y* column index signifies the class index. An object belonging to class *i* thus contains 1 in column *i* for the matrix of dependent variables, and all other columns are zero. The PLSR algorithm computes latent variables that are directed along the maximum *X–Y* covariance (10). In prediction, the class memberships are determined from which *Y* column index corresponds to the largest value.

The *k*-NN method was used as a reference method to DPLSR. From Image 1, spectra of each class were extracted and averaged. This produced five mean spectra, each representing the center point for each class. Classification is based on finding which mean vector has the lowest SAM value to an input test spectrum.

The SAM measure is based on calculating the angle between two spectra represented as the vectors s_1 and s_2. This is to minimize the effect of variation of illumination on the spectra. The SAM distance measure d is defined as $d = \cos^{-1}(s_1^T s_2/(\|s_1\| \|s_2\|))$.

By default, DPLSR or *k*-NN will force a new spectrum to be a member of one of the *k* classes. This is undesirable for cases where a spectrum belonging to an unknown class is encountered. In such a case, the new spectrum should not be assigned to any of the tablet classes. To rectify this problem, the class prediction from DPLSR or *k*-NN is further checked by calculating the Mahalanobis (11) distance from the center of class *k* to the new spectrum. If this distance is too large, the membership will be changed into the background class, which means it will not be shown in the projection. The Mahalanobis cut-off values for each class have here been determined by visual inspection of predicted chemical images where the positions of the class pixels are known.

Validation

It is common to make use of cross-validation or independent test sets to validate classification models. Because hyperspectral images contain a large number of spectra, we have chosen to use independent test set validation. Here, the following validation procedure will only be used for the DPLSR method. The validation approach being taken here can be explained as follows:

- A hyperspectral image (here Image 1) containing the different classes are split into two different subsets. The split is performed by randomly assigning spectra to the different subsets. The first data set (*A*) contains 60% of all the spectra, the second (*B*) contains 40%.
- Data set *A* is the calibration set on which the model parameters are calculated for.
- Data set *B* is used as an independent validation set to determine the optimal number of PLSR factors.
- Image 2 is used as a separate (and independent) test set onto which the optimal PLSR model is applied.

The predictive ability of PLSR models based on $a = 1, 2, \ldots, A_{max}$ factors is determined on 1500 randomly selected spectra (with replacement) from data set *B*. This is performed 30 times for each factor. The prediction error is recorded as the percentage of class predictions that were wrong. A_{opt} corresponds to the optimal model which has the smallest error. The maximum number of PLSR factors tested for A_{max} is set to 20. In addition to the automatic determination of the optimal number of PLSR factors above, we also make use of visual inspection of the predicted class regions. For hyperspectral images with known class regions, visual inspection of the results effectively determines whether the prediction model is successful or not.

Setup and Analysis

All prediction models were constructed using Matlab 7.1 running on both Windows XP and Linux operating systems (Ubuntu, http://www.ubuntu.com). The Windows platform is used for the direct

control and operation of the PryJector instrument. All off-line analyses are performed on Linux workstations using in-house chemometric software.

After inspecting the spectra for the different classes, it became clear that significant area variations were present. These variations are most likely dominated by differences in concentrations of the compounds and are reduced by normalizing the spectra to unit area.

Results

Representative regions in Image 1 corresponding to the different classes were selected (not shown). This resulted in 35,498 spectra that were randomly split into two data sets *A* and *B*. Data set *A* contains 21,299 spectra and data set *B* 14,199. The number of spectra used from Image 2 is 10,626. Both independent test set and visual inspection validation methods produce the same result: A_{opt} = 4 optimal PLSR factors are needed for classification.

The overall prediction error for the test set (Image 2) is 1.4%. The errors for the individual classes are as follows: 0.4% for class 1, 0.8% for class 2, 5.2% for class 3, 0.0% for class 4, and 1.3% for class 5, that is, the background.

The predicted values for all the pixels in Image 1 and 2 are seen in Fig. 3. A PCA of the normalized spectra for the calibration data set confirms the highly predictive model that all the classes are well separated from each other, see Fig. 4.

The corresponding error of using the simplified *k*-NN classification method on Image 2 is 1.6%. The errors for the individual classes are as follows: 0.1% for class 1, 2.5% for class 2, 7.4% for class 3, 0.7% for class 4, and 1.1% for class 5. The result of applying the simplified *k*-NN classification method to the whole of the test image (Image 2) shows that it is comparable to PLSR in its prediction ability. An advantage with the *k*-NN method is that it was not necessary to perform any normalization prior to calculating the class memberships. In real-time applications, any reduction in the needed computation is an advantage.

In Fig. 5, the PLSR model is applied to a simulated situation where the PryJector is used to discover the presence of hidden pharmaceuticals. Here, eight white Paracet tablets are hidden underneath a covering layer of powdered sucrose. A brush is used to uncover the tablets. Figure 5 shows hyperspectral recordings at four different instances in time. The four panels show how the brush is increasingly uncovering more hidden Paracet tablets as is indicated by the projected red color. The panel sequence demonstrates the intended interactivity with the PryJector. Because of current limitations in hardware, each panel is not recorded in real time, but over a interval of *c.* 10 sec, which still allows for interactive investigation of the scene.

Figure 6 shows how a PryJector projection appears to a user when handling powders of various pharmaceuticals, in this case Paracet (red color) and Pamol Smelt (green color). The left panel displays the white powders without using the PryJector, and it appears to the human eye as if only one kind of pharmaceutical is present. However, when the PryJector is switched on (see right panel in Fig. 6), the spatial distribution of the two different types of pharmaceuticals is clearly revealed. Because of a combination of projector misalignment and a shadow effect, regions along the rim of the powder distributions are not highlighted.

Discussion

The table top PryJector instrument has been demonstrated to successfully visualize to the user *in situ* localization of various properties (chemical, physical, or biological). In the application presented, different pharmaceuticals that would for the naked eye be indistinguishable were identified and highlighted on a table.

Given that the compounds or properties of interest can be detected by the hyperspectral camera and modeled using chemometric methods, it is expected that the PryJector approach will be useful for many forensic applications involving manual interaction with surfaces. Of particular interest is using the instrument for improving the manual inspection of clothes and other objects

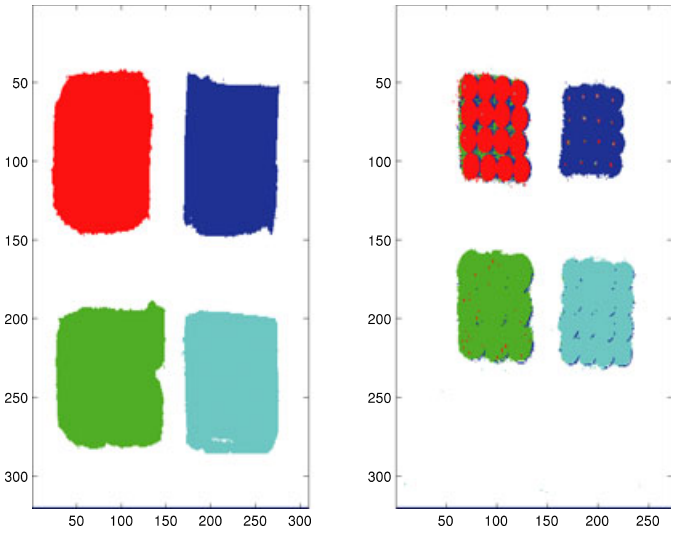

FIG. 3—*The optimal discriminant partial least squares (DPLSR) model is here applied to all pixels in test set image (Image 2) showing the pharmaceuticals in tablet form (right panel). Left panel shows the DPLSR model applied to all pixels, the hyperspectral image used in the calibration (Image 1), see also Fig. 2. Only a subset of the pixels in this image were used as calibration data set.*

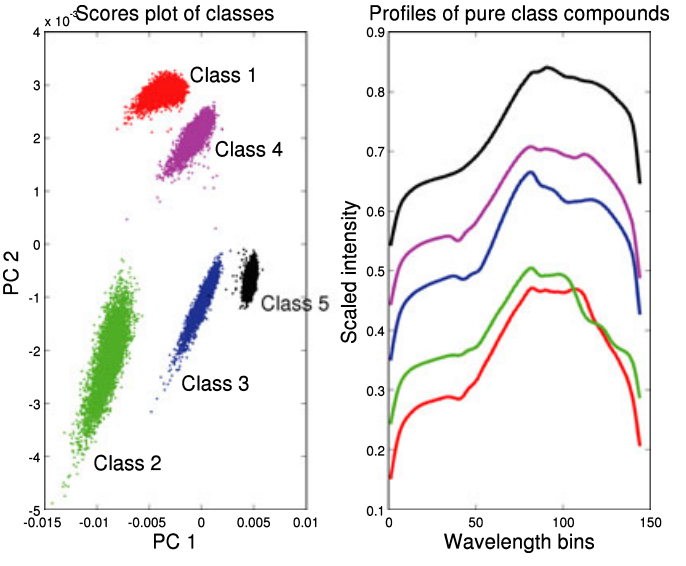

FIG. 4—*The left panel shows the scores plot of the two first principal components of the normalized spectra. As can be seen, the different classes are well separated. The right panel shows the corresponding mean spectra for each class (offset values are added to each spectrum for visualization purposes). Color coding is the same as for left panel: red is class 1, green is class 2, blue is class 3, magenta is class 4, and black is class 5 (the background).*

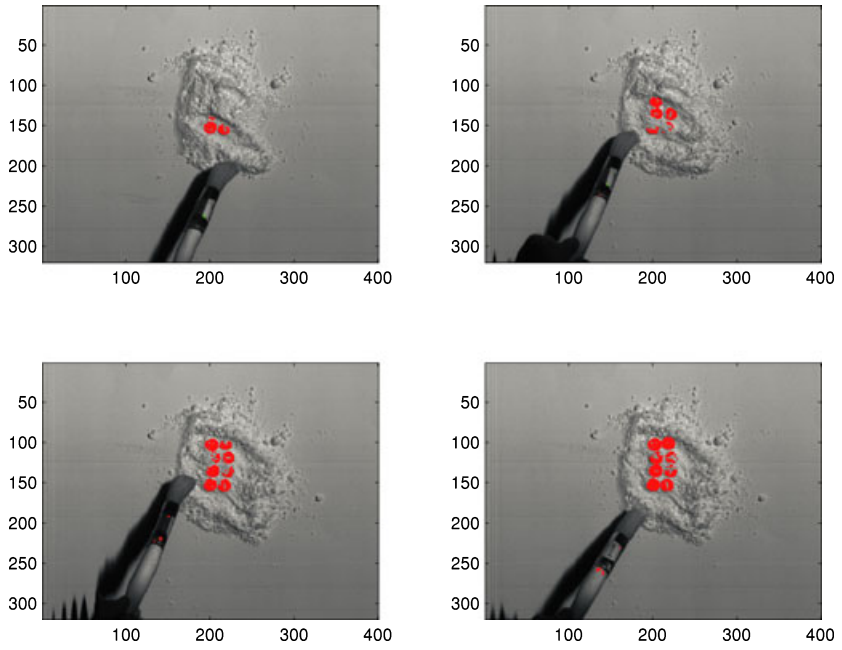

FIG. 5—*The optimal discriminant partial least squares model is here applied to a mix of powdered sugar and one of the tablets types used (Paracet). Eight white Paracet tablets are initially hidden beneath a layer of powdered sugar. By manually using a brush, sugar powder is gradually removed, and the Paracet is made interactively visible by the PryJector by projecting red colored light to pixels identified as belonging to the Paracet class. The sequence of images from upper left to bottom right shows how the Paracet tablet gradually becomes uncovered.*

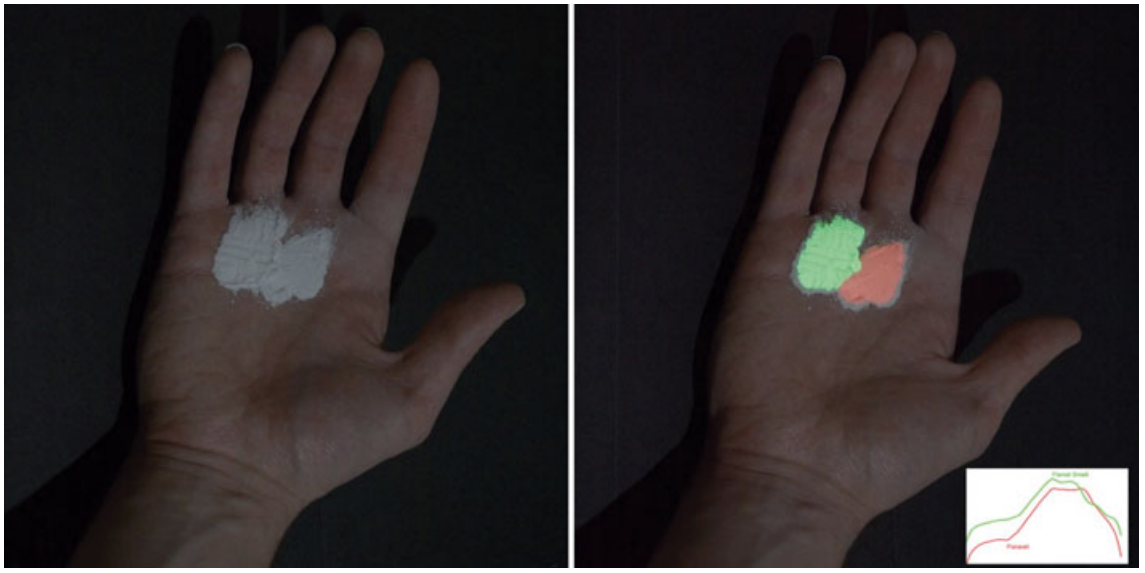

FIG. 6—*Prediction of tablet powder on a human hand. Left panel shows white powder without using the PryJector. Right panel shows how the PryJector visualizes the types of compounds present in the powder. Paracet (red color) and Pamol Smelt (green color) powders are both present. The unclassified regions along the rim of the powder distributions are as a result of shadow effects and misalignment between camera and projector.*

placed on a table. Because the investigator can rapidly switch between a wide range of different chemometric models or automatically search in a database of spectral signatures of interesting compounds, the PryJector facilitates the search for various biological and/or chemical traces that are relevant to an investigation. The PryJector could also be useful for *in situ* fingerprint enhancement. The literature contains several reports on how chemical imaging can be used for this purpose, however, without the dynamic scanning and projection provided by the PryJector. This could enable rapid inspection of larger areas. Similarly, detection and visualization of shoe marks may also be possible. Other applications may be for highlighting marks and bruises on the skin. In other studies (37–39), it is shown how spectroscopy in combination with mathematical modeling can be used to predict the age of bruises. It may therefore be possible to use chemical imaging to enhance/visualize bruises that are either invisible or difficult to detect by the naked eye. Another forensic application of the PryJector is to facilitate the detection and visualization of bone fragments on the ground.

Preliminary results with dried animal bones demonstrate that this is indeed possible.

Two other potential application areas for the PryJector are the medical and defense/security fields. For instance, in medicine, rapid inspection of the skin for cancer and tissue changes may be possible. The instrument might also be helpful during surgery to visualize the presence of cancers or toxic levels of various compounds. In the military field, the PryJector might be used for localization of explosives and other dangerous materials. This would call for an extension of the instrument to scan larger 3D areas for both in- and outdoor conditions. Such an extension of the instrument is indeed possible, however places a much greater demand on the multivariate modeling, as well as the optical design. Various physical and optical effects in the scene can cause the multivariate models to fail, and therefore, new methods may be needed to handle this.

Conclusion

The results of our experiments show that the PryJector instrument facilitates manual inspection of a surface by dynamically projecting the distribution of chemical and physical property distributions onto the same surface. In this respect, the PryJector provides information about target properties visually in a way which is similar to what is seen in traditional forensic methods such as using, for example, chemiluminescent dyes to highlight the distribution of blood on surfaces. However, in contrast to the traditional methods, the PryJector is very flexible with respect to new target properties to search for and highlight on surfaces. This is because of the fact that the instrument is based on creating selectivity to target properties by multivariate and chemometric modeling.

Acknowledgment

Einar Ryeng is thanked for helping the authors to obtain some of the color photographs.

References

1. Lytle LT, Hedgecock DG. Chemiluminescence in visualization of forensic bloodstains. J Forensic Sci 1978;23(3):550–62.
2. Baxter SJ, Rees B. Identification of saliva in stains in forensic casework. Med Sci Law 1975;15(1):37–41.
3. Vandenberg N, Oorschot RAH. The use of polilight in the detection of seminal fluid, saliva, and bloodstains and comparison with conventional chemical-based screening tests. J Forensic Sci 2006;51(2):361–70.
4. Francis PS, Adcock JL, Costin JW, Purcell SD, Pfeffer FM, Barnett NW. Chemiluminescence detection of opium poppy (*Papaver somniferum*) alkaloids. J Pharm Biomed Anal 2008;48(3):508–18.
5. Zoja R, Lazzaro A, Battistini A, Gentile G. Detection of gunshot residues on cadaveric skin using sodium rhodizonate and a counterstain. Biotech Histochem 2006;81(4–6):151–6.
6. Reis ELT, Sarkis JES, Neto ON, Rodrigues C, Kakazu MH, Viebig S. A new method for collection and identification of gunshot residues from the hands of shooters. J Forensic Sci 2003;48(6):1269–74.
7. Stein KM, Bahner ML, Merkel J, Ain S, Mattern R. Detection of gunshot residues in routine cts. Int J Legal Med 2000;2(1–2):15–8.
8. Jackson D, Hadi S. Commentary on: Vandenberg N, van Oorshcot RAH. The use of polilight in the detection of seminal fluid, saliva, and bloodstains and comparison with conventional chemical-based screening tests. J Forensic Sci 2007;52(3):740.
9. Barni F, Lewis SW, Berti A, Miskelly GM, Lago G. Forensic application of the luminol reaction as a presumptive test for latent blood detection. Talanta 2007;72(3):896–913.
10. Martens H, Naes T. Multivariate calibration. New York, NY: John Wiley & Sons, 1989.
11. Massart DL, Vandeginste BGM, Buydens LMC, Jong SD, Lewi PJ, Verbeke-Smeyers J. Handbook of chemometrics and qualimetrics: Part A and B. Amsterdam, the Netherlands: Elsevier Science, 1997.
12. Gupta N. Acousto-optic-tunable-filter-based spectropolarimetric imagers for medical diagnostic applications—instrument design point of view. J Biomed Opt 2005;10(5):051802-1-6.
13. Chang IC. Acoustooptic tunable filters. Opt Eng 1981;20(6):824–9.
14. Chang IC. Tunable acoustooptic filters—overview. Opt Eng 1977;16(5):455–60.
15. Morris HR, Hoyt CC, Treado PJ. Imaging spectrometers for fluorescence and raman microscopy—acoustooptic and liquid-crystal tunable filters. Appl Spectrosc 1994;48(7):857–66.
16. Hardeberg JY, Schmitt F, Brettel H. Multispectral color image capture using a liquid crystal tunable filter. Opt Eng 2002;41(10):2532–48.
17. Morris HR, Hoyt CC, Miller P, Treado PJ. Liquid crystal tunable filter raman chemical imaging. Appl Spectrosc 1996;50(6):805–11.
18. Patel JS. Polarization insensitive tunable liquid-crystal etalon filter. Appl Phys Lett 1991;59(11):1314–6.
19. Wu ST. Design of a liquid-crystal based tunable electrooptic filter. Appl Opt 1989;28(1):48–52.
20. Tahtouh M, Despland P, Shimmon R, Kalman JR, Reedy BJ. The application of infrared chemical imaging to the detection and enhancement of latent fingerprints: method optimization and further findings. J Forensic Sci 2007;52(5):1089–96.
21. Ng PHR, Walker S, Tahtouh M, Reedy B. Detection of illicit substances in fingerprints by infrared spectral imaging. Anal Bioanal Chem 2009;394(8):2039–48.
22. Payne G, Reedy B, Lennard C, Comber B, Exline D, Roux C. A further study to investigate the detection and enhancement of latent fingerprints using visible absorption and luminescence chemical imaging. Forensic Sci Int 2005;150(1):33–5.
23. Exline DL, Wallace C, Roux C, Lennard CI, Nelson MP, Treado PJ. Forensic applications of chemical imaging: latent fingerprint detection using visible absorption and luminescence. J Forensic Sci 2003;48(5):1047–53.
24. Emmons ED, Tripathi A, Guicheteau JA, Christesen SD, Fountain AW. Raman chemical imaging of explosive-contaminated fingerprints. Appl Spectrosc 2009;63(11):1197–203.
25. Flynn K, O'Leary R, Roux C, Reedy BJ. Forensic analysis of bicomponent fibers using infrared chemical imaging. J Forensic Sci 2006;51(3):586–96.
26. Bojko K, Roux C, Reedy BJ. An examination of the sequence of intersecting lines using attenuated total reflectance-fourier transform infrared spectral imaging. J Forensic Sci 2008;53(6):1458–67.
27. Payne G, Wallace C, Reedy B, Lennard C, Schuler R, Exline D, et al. Visible and near-infrared chemical imaging methods for the analysis of selected forensic samples. Talanta 2005;67(2):334–44.
28. Kalacska ME, Bell LS, Sanchez-Azofeifa G, Caelli T. The application of remote sensing for detecting mass graves: an experimental animal case study from Costa Rica. J Forensic Sci 2009;54(1):159–66.
29. Wolfe J, Exline DL. Characterization of condom lubricant components using raman spectroscopy and raman chemical imaging. J Forensic Sci 2003;48(5):1065–74.
30. Lee E, Kidder LH, Kalasinsky VF, Schoppelrei JW, Lewis EN. Forensic visualization of foreign matter in human tissue by near-infrared spectral imaging: methodology and data mining strategies. Cytometry 2006;8(Pt A, 69A):888–96.
31. Brewer LN, Ohlhausen JA, Kotula PG, Michael JR. Forensic analysis of bioagents by X-ray and ToF-SIMS hyperspectral imaging. Forensic Sci Int 2008;179(2–3):98–106.
32. Hemmila A, McGill J, Ritter D. Fourier transform infrared reflectance spectra of latent fingerprints: a biometric gauge for the age of an individual. J Forensic Sci 2008;53(2):369–76.
33. Fernandez FM, Green MD, Newton PN. Prevalence and detection of counterfeit pharmaceuticals: a mini review. Ind Eng Chem Res 2008;47:585–90.
34. Ricci C, Nyadong L, Fernandez FM, Newton PN, Kazarian SG. Combined fourier-transform infrared imaging and desorption electrospray-ionization linear ion-trap mass spectrometry for analysis of counterfeit antimalarial tablets. Anal Bioanal Chem 2007;387:551–9.
35. Duda RO, Hart PE, Stork DG. Pattern classification, 2nd edn. New York, NY: Wiley-Interscience, 2002.
36. Kruse FA, Lefkoff AB, Boardman JW, Heidebrecht KB, Shapiro AT, Barloon PJ, et al. The spectral image-processing system (sips)—

interactive visualization and analysis of imaging spectrometer data. Remote Sens Environ 1993;44(2–3):145–63.
37. Payne G, Langlois N, Lennard C, Roux C. Applying visible hyperspectral (chemical) imaging to estimate the age of bruises. Med Sci Law 2007;47(3):225–32.
38. Randeberg LL, Haugen OA, Haaverstad R, Svaasand LO. A novel approach to age determination of traumatic injuries by reflectance spectroscopy. Lasers Surg Med 2006;38(4):277–89.
39. Randeberg LL, Winnem AM, Langlois NE, Larsen ELP, Haaverstad R, Skallerud B, et al. Skin changes following minor trauma. Lasers Surg Med 2007;39(5):403–13.

Additional information and reprint requests:
Bjørn Kåre Alsberg, Ph.D.
Professor
Department of Chemistry
Norwegian University of Science and Technology (NTNU)
Høgskoleringen 5d
N-7491, Trondheim
Norway
E-mail: alsberg@nt.ntnu.no